

Numerical Methods for Coupled Surface and Grain Boundary Motion

Zhenguo Pan , Brian Wetton

Department of Mathematics, University of British Columbia,
Vancouver, B.C. Canada

Abstract

We study the coupled surface and grain boundary motion in a bicrystal in the context of the “quarter loop” geometry. Two types of physics motions are involved in this model: motion by mean curvature and motion by surface diffusion. The goal is finding a formulation that can describe the coupled motion and has good numerical behavior when discretized. Two formulations are proposed in this paper. One of them is given by a mixed order parabolic system and the other is given by Partial Differential Algebraic Equations. The parabolic formulation constitutes several parabolic equations which model the two normal direction motions separately. The performance of this formulation is good for a short time simulation. It performs even better by adding an extra term to adjust the tangential velocity of grid points. The PDAE formulation preserves the scaled arc length property and performs much better with no need to add an adjusting term. Both formulations are proven to be well-posed in a simpler setting and are solved by finite difference methods.

Key words: Grain Boundary; Mean Curvature Motion; Surface Diffusion; Well-posedness; Finite Difference

1 Introduction

Coupled surface and grain boundary motion is an important phenomenon controlling the grain growth in materials processing and synthesis. A commonly used model to study this coupled effect is called “quarter loop” geometry introduced by Dunn et al. [6].

In the quarter loop geometry, there are two grains between which there is an interface called grain boundary as shown in Fig.1. The two grains are of the same material and differ only in their relative crystalline orientation. The grain boundary runs parallel to a free surface before it turns up and attaches to upper surfaces at a groove root. When heated at a specific temperature, the grain boundary migrates to reduce the surface energy and to heal the orientation mismatch. Since the driving force is constant the grain boundary moves at a constant velocity after a short time

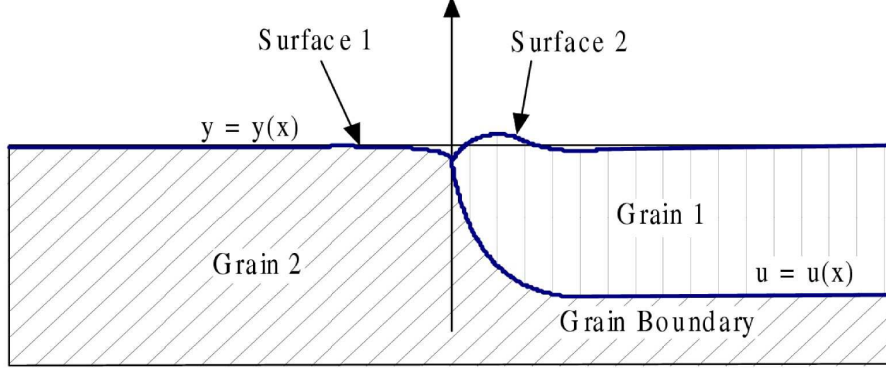


Figure 1: The quarter loop bicrystal geometry.

decay. It is reasonable to assume that the bicrystal is uniform along the cross-section direction. Thus it is reasonable for us to consider only two dimensional(2D) geometry in this paper.

This geometry contains two types of motion. One of them is mean curvature motion for the grain boundary. And the other one is surface diffusion for the upper surfaces. More detail about this model is give in [10].

Motion by mean curvature is an evolution law in which the normal velocity of an interface is proportional to its mean curvature. More precisely, the motion of an interface Γ satisfies

$$V_c = A\kappa \quad (1)$$

Here V_c denotes the velocity in the normal direction of Γ , and κ stands for the mean curvature of Γ .

First proposed by Mullins [13] to model the curvature driven diffusion on the surface of a crystal, surface diffusion is a different evolution law in which the normal velocity of an interface is proportional to the surface Laplacian of mean curvature. The motion of interface Γ satisfies

$$V_d = -B\Delta_s\kappa \quad (2)$$

Here V_d stands for the normal velocity and Δ_s stands for the operator of surface Laplacian which is defined as

$$\Delta_s = \nabla_s \cdot \nabla_s \text{ where } \nabla_s = \nabla - n\partial_n \quad (3)$$

In two dimensions, surface diffusion can be reduced to a normal direction motion with a speed function depending on the second derivative of the curvature with respect to arc length, i.e.,

$$V_d = -B\kappa_{ss} \quad (4)$$

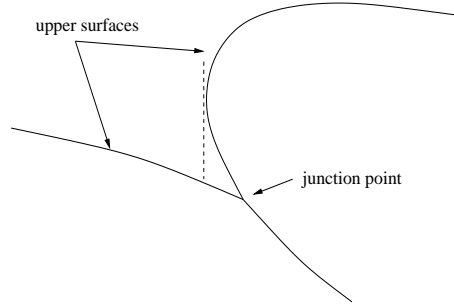


Figure 2: An example when one of the surfaces is not single-valued.

Here s is arc length parametrization. Since the problem is proposed in two dimensions, the motion by surface diffusion always refers to equation (4) instead of the general case (2) in this paper.

We shall prove later in the appendix that we could normalize A and B by rescaling the time and space. Since this reformulation make the problem neither harder or easier we will take both A and B as one.

Surface diffusion is an intrinsically difficult problem to solve numerically even in two dimensions. The main difficulty is that it is stiff due to the fourth order derivatives and such that an explicit time stepping strategy requires very small time steps. Moreover, owing to the lack of a maximum principle, an embedded curve may not stay embedded, in other words, it may become self-intersected during the evolution.

Travelling wave solutions have been derived for the whole nonlinear problem and for a linearized problem in [11] and [10] respectively. These analytic results are used to verify numerical results in this paper.

The formulations in this paper will be proposed in parameterized form. There are two reasons why we prefer the parameterized form. Firstly, we try to set up a versatile formulation that is extensible to other problems, such as the evolution of a closed curve, other freely positioned triple junction problems and even the evolution curve networks, wherever for a single type motion or a mixed type motion. Secondly, even for the coupled grain boundary motion, the function $y(x)$ which represents the exterior surface may not be single-valued as shown in Fig.2 and this phenomena is physically reasonable [8, 9]. Also for such consideration we will treat the exterior surface as two curves separated by the triple junction in the following discussion.

The outline of this paper is as follows. In section 3, parabolic equations are derived for the motion by mean curvature and the motion by surface diffusion separately. The boundary conditions including the triple junction conditions and domain boundary conditions are discussed in section 4 referring to the analytic work of Novick-Cohen et al. [10, 11] and Wong et al. [12]. In section 5, the well-posedness for a linear parabolic system that is closely related to the full nonlinear problem is analyzed and followed by a discussion about the artificial tangential condition. From section 6 to 8

we discuss the numerical details including discretization, time stepping and some other numerical issues. We start the discussion for a PDAE system in section 9. An interesting computational example of surface diffusion is given in section 10. The linear well-posedness of the PDAE system is analyzed in section 11.

2 Cartesian Formulation

In this section, we consider the problem in the cartesian coordinate system which is give as below(see [10]).

$$\begin{aligned} y_t &= -\left[\frac{1}{(1+y_x^2)^{1/2}}\left[\frac{y_{xx}}{(1+y_x^2)^{3/2}}\right]_x\right]_x, \quad t > 0, x \in (-\infty, s(t)^-) \cup (s(t)^+, \infty), \\ u_t &= u_{xx}(1+u_x^2)^{-1}, \quad t > 0, x > s(t) \end{aligned} \quad (5)$$

with following triple junction conditions

$$\begin{aligned} y(s(t)^+, t) &= y(s(t)^-, t) = u(s(t)^+, t), \quad t > 0 \\ \arctan(y_x(s(t)^+, t)) - \arctan(y_x(s(t)^-, t)) &= 2 \arcsin\left(\frac{\gamma_{\text{grain}}}{2\gamma_{\text{exterior}}}\right) \\ \arctan(u_x(s(t)^+, t)) &= -\frac{\pi}{2} + \frac{1}{2}[\arctan(y_x(s(t)^+, t)) + \arctan(y_x(s(t)^-, t))], \quad t > 0 \\ \frac{y_{xx}}{(1+y_x^2)^{3/2}}\Big|_{(s(t)^+, t)} &= \frac{y_{xx}}{(1+y_x^2)^{3/2}}\Big|_{(s(t)^-, t)}, \quad t > 0 \\ \left[\frac{1}{(1+y_x^2)^{1/2}}\left[\frac{y_{xx}}{(1+y_x^2)^{3/2}}\right]_x\right]_{(s(t)^+, t)} &= \left[\frac{1}{(1+y_x^2)^{1/2}}\left[\frac{y_{xx}}{(1+y_x^2)^{3/2}}\right]_x\right]_{(s(t)^-, t)}, \quad t > 0 \\ y(+\infty, t) &= y(-\infty, t) = 0, \quad t > 0 \\ u(+\infty, t) &= -1, \quad t > 0 \end{aligned} \quad (6)$$

Here $y = y(x, t)$ stands for the height of the two exterior surfaces. $u = u(x, t)$ is the height of the grain boundary and $s(t)$ denotes the location of the junction where the three surfaces meet.

Since the junction is moving it is not straightforward to solve this system numerically. We fix the junction by making the following transform,

$$\bar{x} = x - s(t) \quad (7)$$

We let $y(\bar{x}, t) = y(x, t)$ and $u(\bar{x}, t) = u(x, t)$. Therefor,

$$\begin{aligned} y_x(x, t) &= y_{\bar{x}}(\bar{x}, t) \\ y_t(x, t) &= y_t(\bar{x}, t) - y_{\bar{x}}(\bar{x}, t)s_t \\ u_x(x, t) &= u_{\bar{x}}(\bar{x}, t) \\ u_t(x, t) &= u_t(\bar{x}, t) - u_{\bar{x}}(\bar{x}, t)s_t \end{aligned}$$

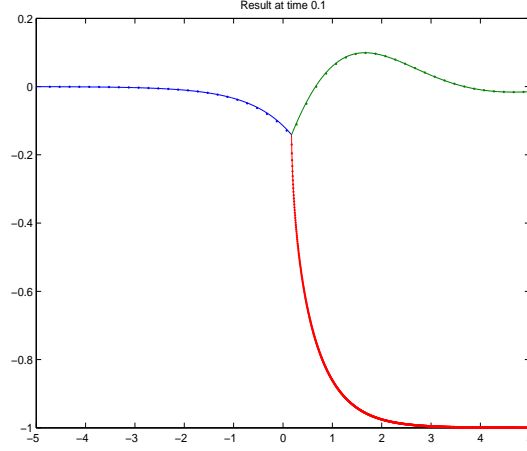


Figure 3: Numerical result for system (8)-(9) with $m = 0.5$. Dotted line: numerical result; Solid line: travelling wave solution.

Then system (5) becomes

$$\begin{aligned} y_t &= -\left[\frac{1}{(1+y_{\bar{x}}^2)^{1/2}}\left[\frac{y_{\bar{x}\bar{x}}}{(1+y_{\bar{x}}^2)^{3/2}}\right]_{\bar{x}}\right]_{\bar{x}} + y_{\bar{x}}(\bar{x}, t)s_t, \quad t > 0, \bar{x} \in (-\infty, 0) \cup (0, \infty), \\ u_t &= u_{\bar{x}\bar{x}}(1+u_{\bar{x}}^2)^{-1} + y_{\bar{x}}(\bar{x}, t)s_t, \quad t > 0, \bar{x} > 0 \end{aligned} \quad (8)$$

And the boundary conditions (6) become

$$\begin{aligned} y(0^+, t) &= y(0^-, t) = u(0^+, t), \quad t > 0 \\ \arctan(y_{\bar{x}}(0^+, t)) - \arctan(y_{\bar{x}}(0^-, t)) &= 2 \arcsin\left(\frac{\gamma_{\text{grain}}}{2\gamma_{\text{exterior}}}\right) \\ \arctan(u_{\bar{x}}(0^+, t)) &= -\frac{\pi}{2} + \frac{1}{2}[\arctan(y_{\bar{x}}(0^+, t)) + \arctan(y_{\bar{x}}(0^-, t))], \quad t > 0 \\ \frac{y_{\bar{x}\bar{x}}}{(1+y_{\bar{x}}^2)^{3/2}}\Big|_{(0^+, t)} &= \frac{y_{\bar{x}\bar{x}}}{(1+y_{\bar{x}}^2)^{3/2}}\Big|_{(0^-, t)}, \quad t > 0 \\ \left[\frac{1}{(1+y_{\bar{x}}^2)^{1/2}}\left[\frac{y_{\bar{x}\bar{x}}}{(1+y_{\bar{x}}^2)^{3/2}}\right]_{\bar{x}}\right]_{(0^+, t)} &= \left[\frac{1}{(1+y_{\bar{x}}^2)^{1/2}}\left[\frac{y_{\bar{x}\bar{x}}}{(1+y_{\bar{x}}^2)^{3/2}}\right]_{\bar{x}}\right]_{(0^-, t)}, \quad t > 0 \\ y(+\infty, t) &= y(-\infty, t) = 0, \quad t > 0 \\ u(+\infty, t) &= -1, \quad t > 0 \end{aligned} \quad (9)$$

This system could easily be discretized using standard finite difference schemes on a fixed staggered grid. A numerical result is shown in Fig.3.

The disadvantage of using cartesian formulation is that it is not applicable to non-single valued case as shown in Fig.2. What's more, since the grain boundary is nearly singular at the junction, it requires very small grid size for accuracy. For wider application we consider two parametric formulations in the rest of this paper.

3 A Parabolic Formulation

In this section we derive a parabolic system to model the coupled motion. Here and throughout this paper we use $X = (u(\cdot), v(\cdot))$ to represent a parameterized curve with $u(\cdot)$ and $v(\cdot)$ being the coordinates.

Several more notations should be introduced as well. The arc length parameter is denoted by $X(s) = X(u(s), v(s))$ and any other parameter is denoted by $X(\sigma) = X(u(\sigma), v(\sigma))$. \vec{t} and \vec{n} stand for unit tangential direction and unit normal direction respectively. κ stands for curvature. Although all final equations are parameterized by σ , the arc length parametrization is useful for the intermediate deviations.

3.1 Motion by Mean Curvature

We first derive a parabolic equation to describe the motion by mean curvature. Similar discussion has been addressed in [3] and [7]. We give a brief description for reader's convenience.

With the notations introduced above one has

$$X_s = \vec{t}$$

$$X_{ss} = \kappa \vec{n}$$

Here the subscript s stands for the derivative of X with respect to arc length s . Direct computation shows that

$$X_\sigma = X_s \frac{dS(\sigma)}{d\sigma} = X_s |X_\sigma| \quad (10)$$

where $S(\sigma)$ is defined by

$$S(\sigma) = \int_{\sigma_0}^{\sigma} \sqrt{u_\sigma^2 + v_\sigma^2} d\sigma \quad (11)$$

which stands for the length of the curve from point $X(\sigma_0)$ to $X(\sigma)$. $|X_\sigma|$ is L_2 norm of X_σ defined by

$$|X_\sigma| = \sqrt{u_\sigma^2 + v_\sigma^2}$$

Differentiate equation (10) with respect to σ to obtain

$$X_{\sigma\sigma} = X_{ss}|X_\sigma|^2 + X_s|X_\sigma|_s|X_\sigma| \quad (12)$$

By previous derivations one can compute the normal component of vector $\frac{X_{\sigma\sigma}}{|X_\sigma|^2}$ and obtains

$$\begin{aligned} \frac{X_{\sigma\sigma}}{|X_\sigma|^2} \cdot \vec{n} &= X_{ss} \cdot \frac{X_{ss}}{\kappa} + \frac{|X_\sigma|_s}{|X_\sigma|} X_s \cdot \frac{X_{ss}}{\kappa} \\ &= \kappa \end{aligned} \quad (13)$$

Thus, if we set up a formulation:

$$X_t = \frac{X_{\sigma\sigma}}{|X_\sigma|^2} \quad (14)$$

it is obvious that the motion described by (14) has normal velocity κ . This gives us an option to describe the motion by mean curvature. Equation (14) is fully parabolic which means it is parabolic in both the normal component and tangential component.

There are some other equations that can also describe curvature motion, for example,

$$X_t = \kappa \vec{n} \quad (15)$$

But this system is not fully parabolic. A linearization shows that this system is parabolic in the normal component and hyperbolic in the tangential component. A discretization of system (15) will not have the good numerical properties as those of a fully parabolic system due to the lack of regularity in the parametrization as shown in [3].

3.2 Motion by Surface Diffusion

Considering the good properties of a parabolic formulation, we hope to find a parabolic formulation for motion by surface diffusion. By analogy with the approach to the mean curvature motion described above, we try the following form:

$$X_t = -\frac{X_{\sigma\sigma\sigma\sigma}}{|X_\sigma|^4} + L(X_{\sigma\sigma\sigma}, X_{\sigma\sigma}, X_\sigma) \quad (16)$$

where $L(X_{\sigma\sigma\sigma}, X_{\sigma\sigma}, X_\sigma)$ includes some lower order terms and will be determined such that

$$X_t \cdot \vec{n} = \left(-\frac{X_{\sigma\sigma\sigma\sigma}}{|X_\sigma|^4} + L(X_{\sigma\sigma\sigma}, X_{\sigma\sigma}, X_\sigma)\right) \cdot \vec{n} = -\kappa_{ss} \quad (17)$$

We focus our study on finding out $L(X_{\sigma\sigma\sigma}, X_{\sigma\sigma}, X_\sigma)$ in the rest of this section.

Note first the following equation (see appendix for proof),

$$(X_{ssss} + \kappa^2 X_{ss}) \cdot \vec{n} = \kappa_{ss} \quad (18)$$

Compare equation (17) and (18) to get a choice for L ,

$$L(X_{\sigma\sigma\sigma}, X_{\sigma\sigma}, X_\sigma) = \frac{X_{\sigma\sigma\sigma\sigma}}{|X_\sigma|^4} - X_{ssss} - \kappa^2 X_{ss} \quad (19)$$

One will find later that the fourth order terms appeared in (19) could be cancelled with each other and such that L involves only third or lower order derivatives.

Start by equation (10) and differentiate several times with respect to σ to get following relations,

$$X_{\sigma\sigma} = X_{ss}S_\sigma^2 + X_s S_{\sigma\sigma} \quad (20)$$

$$X_{\sigma\sigma\sigma} = X_{sss}S_\sigma^3 + 3X_{ss}S_\sigma S_{\sigma\sigma} + X_s S_{\sigma\sigma\sigma} \quad (21)$$

$$X_{\sigma\sigma\sigma\sigma} = X_{ssss}S_\sigma^4 + 6X_{sss}S_\sigma^2 S_{\sigma\sigma} + 4X_{ss}S_\sigma S_{\sigma\sigma\sigma} + 3X_{ss}S_{\sigma\sigma}^2 + X_s S_{\sigma\sigma\sigma\sigma} \quad (22)$$

Dividing through equation (22) by S_σ^4 and noticing the fact that $|X_\sigma| = S_\sigma$ one obtains

$$\frac{X_{\sigma\sigma\sigma\sigma}}{|X_\sigma|^4} = X_{ssss} + 6\frac{S_{\sigma\sigma}}{S_\sigma^2}X_{sss} + 4\frac{S_{\sigma\sigma\sigma}}{S_\sigma^3}X_{ss} + 3\frac{S_{\sigma\sigma}^2}{S_\sigma^4}X_{ss} + \frac{S_{\sigma\sigma\sigma\sigma}}{S_\sigma^4}X_s \quad (23)$$

Substitute equation (23) into (19), rewrite arc length parametrization s into σ using (20)-(21). Since vector X_s is perpendicular to \vec{n} and has no contribution to normal direction we can ignore all X_s terms and obtain

$$L(X_{\sigma\sigma\sigma}, X_{\sigma\sigma}, X_\sigma) = 6\frac{S_{\sigma\sigma}}{S_\sigma^2}\frac{X_{\sigma\sigma\sigma}}{|X_\sigma|^3} - 15\frac{S_{\sigma\sigma}^2}{S_\sigma^4}\frac{X_{\sigma\sigma}}{|X_\sigma|^2} + 4\frac{S_{\sigma\sigma\sigma}}{S_\sigma^3}\frac{X_{\sigma\sigma}}{|X_\sigma|^2} - \kappa^2\frac{X_{\sigma\sigma}}{|X_\sigma|^2} \quad (24)$$

Substitute equation (24) back into (16) and collect to get the scheme as

$$X_t = -\frac{X_{\sigma\sigma\sigma\sigma}}{|X_\sigma|^4} + 6S_{\sigma\sigma}\frac{X_{\sigma\sigma\sigma}}{|X_\sigma|^5} - (15\frac{S_{\sigma\sigma}^2}{|X_\sigma|^4} - 4\frac{S_{\sigma\sigma\sigma}}{|X_\sigma|^3} + \kappa^2)\frac{X_{\sigma\sigma}}{|X_\sigma|^2} \quad (25)$$

We would like to point out that the choice of L is not unique. A similar expression has been given by Garcke et al. in [7].

3.3 The Parabolic System

We now give the fully parabolic system,

$$\begin{aligned} X_t^1 &= \frac{X_{\sigma\sigma}^1}{|X_\sigma^1|^2} \\ X_t^2 &= -\frac{X_{\sigma\sigma\sigma\sigma}^2}{|X_\sigma^2|^4} + 6S_{\sigma\sigma}\frac{X_{\sigma\sigma\sigma}^2}{|X_\sigma^2|^5} - (15\frac{S_{\sigma\sigma}^2}{|X_\sigma^2|^4} - 4\frac{S_{\sigma\sigma\sigma}}{|X_\sigma^2|^3} + \kappa^2)\frac{X_{\sigma\sigma}^2}{|X_\sigma^2|^2} \\ X_t^3 &= -\frac{X_{\sigma\sigma\sigma\sigma}^3}{|X_\sigma^3|^4} + 6S_{\sigma\sigma}\frac{X_{\sigma\sigma\sigma}^3}{|X_\sigma^3|^5} - (15\frac{S_{\sigma\sigma}^2}{|X_\sigma^3|^4} - 4\frac{S_{\sigma\sigma\sigma}}{|X_\sigma^3|^3} + \kappa^2)\frac{X_{\sigma\sigma}^3}{|X_\sigma^3|^2} \end{aligned} \quad (26)$$

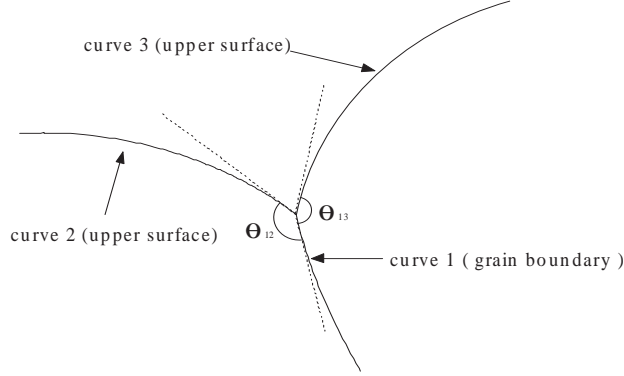


Figure 4: Sketch of the grain boundary groove.

where X^1 stands for the grain boundary and X^2, X^3 stand for the left branch and right branch of the upper surface respectively. All curves are represented by $X(\sigma)$ with $\sigma \in [0, \infty)$.

This system will be solved numerically with the boundary conditions discussed in the next section.

4 Boundary Conditions

The grain boundary and the two upper surfaces meet together at one end which is referred as triple junction. The other end of the three curves tends to infinity in the quarter loop geometry. For numerical reasons, we compute this problem in a bounded domain. This domain is chosen large enough such that it can simulate the motion at least for a short time. This restriction is reasonable since the curves are asymptotically flat for the parts far away from the triple junction. All computations presented in this paper are constrained in a finite domain $[-6, 12]$ and the curves are parameterized with $\sigma \in [0, 1]$.

At $\sigma = 0$ the three curves meet at a triple junction and at $\sigma = 1$ the three curves meet the artificial domain boundary separately.

4.1 Triple Junction Conditions at $\sigma = 0$

We first discuss the boundary conditions at the triple junction. First of all, three curves should have common coordinates at $\sigma = 0$, i.e.,

$$X^1(0, t) = X^2(0, t) = X^3(0, t) \quad (27)$$

By Young's law we have two more conditions which are referred as angle conditions:

$$\frac{X_\sigma^1}{|X_\sigma^1|} \cdot \frac{X_\sigma^2}{|X_\sigma^2|} = \cos \theta_{12} = \cos\left(\frac{\pi}{2} + \arcsin \frac{m}{2}\right) \quad (28)$$

$$\frac{X_\sigma^1}{|X_\sigma^1|} \cdot \frac{X_\sigma^3}{|X_\sigma^3|} = \cos \theta_{13} = \cos\left(\frac{\pi}{2} + \arcsin \frac{m}{2}\right) \quad (29)$$

where θ_{ij} denotes the angle between curve i, j and $m = \gamma_{\text{grain}}/\gamma_{\text{exterior}}$ is a constant measuring the relative surface energy between the grain boundary and exterior surface.

The continuity of the surface chemical potentials implies that

$$\kappa^2 = -\kappa^3 \quad \left(\kappa = \frac{X_{\sigma\sigma}}{|X_\sigma|^2} \cdot \frac{X_\sigma^\perp}{|X_\sigma|}\right) \quad (30)$$

Here the superscripts are indices of curves.

And the balance of mass flux implies that

$$\kappa_s^2 = \kappa_s^3 \quad \left(\kappa_s = \frac{X_{\sigma\sigma\sigma} \cdot X_\sigma^\perp}{|X_\sigma|^4} - 3 \frac{|X_\sigma|_\sigma (X_{\sigma\sigma} \cdot X_\sigma^\perp)}{|X_\sigma|^5}\right) \quad (31)$$

where the expression for κ_s is obtained by taking the derivative of the expression of κ directly.

We must be careful about condition (30). Basically, we need the two upper surfaces have the same convexity. Since σ has opposite directions for the two curves the odd time derivatives will have opposite signs when computed by parametric form. Thus we should put a minus sign for (30) and keep the same for (31).

4.2 Boundary Conditions at $\sigma = 1$

At the other ends of the curves we put several artificial conditions such that they do not move during evolution and keep being flat. This is reasonable since they start being flat and they will not be influenced by the motion of the triple junction in a short time. The following conditions are imposed at $\sigma = 1$,

$$\begin{aligned} X_t^i(1, t) &= \mathbf{0} & \text{for } i = 1, 2, 3 \\ X_{\sigma\sigma}^i(1, t) &= \mathbf{0} & \text{for } i = 2, 3 \end{aligned}$$

4.3 Artificial Tangential Conditions

We should point out that the whole system contains two second order equations and four fourth order equations and it should have ten conditions at the junction point for well-posedness. Recall that there are only eight junction conditions as have been addressed above. Thus, we need two more conditions. There are several options to impose the extra conditions. And we will prove later

that different conditions could only change the parametrization of the curves and will not change the profiles of the curves. Since these conditions do change the tangential velocities of the grid nodes we refer them as artificial tangential conditions. As one of the options, the following two conditions are applied into the system:

$$X_{\sigma\sigma}^i \cdot X_\sigma^i = 0 \quad \text{for } i = 2, 3 \quad (32)$$

5 Well-posedness for the Parabolic System

In this section, we analyze the well-posedness of the system proposed above. We linearize around fixed straight line solutions and get a system that has the same highest order parabolic behavior as the original problem. The well-posedness we do gives the conditions that match those that in more complicated nonlinear analysis gives, where such analysis exists. And therefore, we believe the results of the analysis should apply to the full nonlinear problem.

5.1 Linearization of the System

To linearize the system we consider a perturbation expansion around the tangential direction at the triple junction for each curve, i.e.,

$$\begin{aligned} X^1 &= d_1\sigma + \epsilon\bar{X}^1 + O(\epsilon^2) \\ X^2 &= d_2\sigma + \epsilon\bar{X}^2 + O(\epsilon^2) \\ X^3 &= d_3\sigma + \epsilon\bar{X}^3 + O(\epsilon^2) \end{aligned}$$

where $d_i = (d_{i1}, d_{i2})$ is a constant vector standing for the unit tangential direction. Substitute above equations into (26), linearize and keep the leading order terms to get a linear system:

$$\begin{aligned} \bar{X}_t^1 &= \bar{X}_{\sigma\sigma}^1 \\ \bar{X}_t^2 &= -\bar{X}_{\sigma\sigma\sigma}^2 \\ \bar{X}_t^3 &= -\bar{X}_{\sigma\sigma\sigma}^3 \end{aligned} \quad (33)$$

For convenience, we omit the bar above X in following discussion.

The linearization of the triple junction conditions is straightforward.

- Common point at $\sigma = 0$:

$$X^1 = X^2 = X^3$$

- Angle conditions:

$$\begin{aligned} d_1 \cdot X_\sigma^2 + d_2 \cdot X_\sigma^1 - (d_1 \cdot d_2)(d_1 \cdot X_\sigma^1 + d_2 \cdot X_\sigma^2) &= 0 \\ d_1 \cdot X_\sigma^3 + d_3 \cdot X_\sigma^1 - (d_1 \cdot d_3)(d_1 \cdot X_\sigma^1 + d_3 \cdot X_\sigma^3) &= 0 \end{aligned}$$

- Continuity of surface chemical potentials:

$$X_{\sigma\sigma}^2 \cdot d_2^\perp = -X_{\sigma\sigma}^3 \cdot d_3^\perp$$

- Balance of mass flux:

$$X_{\sigma\sigma\sigma}^2 \cdot d_2^\perp = X_{\sigma\sigma\sigma}^3 \cdot d_3^\perp$$

- Artificial tangential conditions:

$$\begin{aligned} X_{\sigma\sigma}^2 \cdot d_2 &= 0 \\ X_{\sigma\sigma}^3 \cdot d_3 &= 0 \end{aligned}$$

The linear system (33) can be solved using Laplace transforms to get

$$\begin{cases} u_1 = A_{11}e^{-\sqrt{s}\sigma} \\ v_1 = A_{12}e^{-\sqrt{s}\sigma} \\ u_2 = A_{21}e^{\lambda_1\sigma} + B_{21}e^{\lambda_2\sigma} \\ v_2 = A_{22}e^{\lambda_1\sigma} + B_{22}e^{\lambda_2\sigma} \\ u_3 = A_{31}e^{\lambda_1\sigma} + B_{31}e^{\lambda_2\sigma} \\ v_3 = A_{32}e^{\lambda_1\sigma} + B_{32}e^{\lambda_2\sigma} \end{cases} \quad (34)$$

where

$$\lambda_1 = \left(-\frac{\sqrt{2}}{2} + \frac{\sqrt{2}}{2}i\right)\sqrt[4]{s} \quad \lambda_2 = \left(-\frac{\sqrt{2}}{2} - \frac{\sqrt{2}}{2}i\right)\sqrt[4]{s}$$

and here s temporally stands for the transformed time variable of Laplace transform.

For simplicity, we first suppose the angles between any two curves are $\frac{2}{3}\pi$. Substituting solution (34) into boundary conditions one obtains a 10×10 coefficient matrix M (transposed)

$$\begin{pmatrix} 1 & 0 & 0 & 0 & (-d_{21} - \frac{1}{2}d_{11})\sqrt{s} & (-d_{31} - \frac{1}{2}d_{11})\sqrt{s} & 0 & 0 & 0 & 0 \\ 0 & 0 & 1 & 0 & (-d_{22} - \frac{1}{2}d_{12})\sqrt{s} & (-d_{32} - \frac{1}{2}d_{12})\sqrt{s} & 0 & 0 & 0 & 0 \\ -1 & 1 & 0 & 0 & (d_{11} + \frac{1}{2}d_{21})\lambda_1 & 0 & -d_{22}\lambda_1^2 & -d_{22}\lambda_1^3 & d_{21}\lambda_1^2 & 0 \\ -1 & 1 & 0 & 0 & (d_{11} + \frac{1}{2}d_{21})\lambda_2 & 0 & -d_{22}\lambda_2^2 & -d_{22}\lambda_2^3 & d_{21}\lambda_2^2 & 0 \\ 0 & 0 & -1 & 1 & (d_{12} + \frac{1}{2}d_{22})\lambda_1 & 0 & d_{21}\lambda_1^2 & d_{21}\lambda_1^3 & d_{22}\lambda_1^2 & 0 \\ 0 & 0 & -1 & 1 & (d_{12} + \frac{1}{2}d_{22})\lambda_2 & 0 & d_{21}\lambda_2^2 & d_{21}\lambda_2^3 & d_{22}\lambda_2^2 & 0 \\ 0 & -1 & 0 & 0 & 0 & (d_{11} + \frac{1}{2}d_{31})\lambda_1 & -d_{32}\lambda_1^2 & d_{32}\lambda_1^3 & 0 & d_{31}\lambda_1^2 \\ 0 & -1 & 0 & 0 & 0 & (d_{11} + \frac{1}{2}d_{31})\lambda_2 & -d_{32}\lambda_2^2 & d_{32}\lambda_2^3 & 0 & d_{31}\lambda_2^2 \\ 0 & 0 & 0 & -1 & 0 & (d_{12} + \frac{1}{2}d_{32})\lambda_1 & d_{31}\lambda_1^2 & -d_{31}\lambda_1^3 & 0 & d_{32}\lambda_1^2 \\ 0 & 0 & 0 & -1 & 0 & (d_{12} + \frac{1}{2}d_{32})\lambda_2 & d_{31}\lambda_2^2 & -d_{31}\lambda_2^3 & 0 & d_{32}\lambda_2^2 \end{pmatrix} \quad (35)$$

Linear well-posedness requires that the determinant of matrix M is nonsingular for any s satisfying $\text{Re}(s) > 0$. Since the well-posedness depends only on their relative positions, we suppose further that

$$d_1 = \begin{pmatrix} 0 \\ -1 \end{pmatrix} \quad d_2 = \begin{pmatrix} -\frac{\sqrt{3}}{2} \\ \frac{1}{2} \end{pmatrix} \quad d_3 = \begin{pmatrix} \frac{\sqrt{3}}{2} \\ \frac{1}{2} \end{pmatrix}$$

With these assumptions, one obtains the determinant of M :

$$|M| = 6\sqrt{6}s^{11/4} + 24\sqrt{3}s^3$$

Similarly the determinant of M for arbitrary angles is

$$|M| = 32(\sin \theta_{13} \sin^2 \theta_{12} + \sin \theta_{12} \sin^2 \theta_{13})s^3 - 16\sqrt{2}(\sin \theta_{12} \sin \theta_{13} \sin(\theta_{12} + \theta_{13}))s^{11/4}$$

where θ_{12}, θ_{13} are the angles between the curves as shown in Fig.4. M is nonsingular for any s with $\text{Re}(s) > 0$ if $0 < \theta_{12}, \theta_{13} < \pi$. The constraint on θ is not an issue since it has included all the cases of interest.

5.2 Analysis of Artificial Tangential Conditions

As have been mentioned before, there are several options for the artificial tangential conditions. We are interested to know if different choices will lead to the same solution which is shown to be true. To prove this point, it suffices to prove that the position of the junction and the three tangential directions do not depend on the artificial tangential conditions. The idea to prove this point is to show that they all lead to the same solution for X_1 . If this is true, the position of the junction point and the tangential direction of X_1 are uniquely determined. Since the angle conditions are guaranteed, the tangential directions of the other two curves could also be uniquely determined. To sum up, the key point is proving coefficients of X^1 , i.e., A_{11}, A_{12} do not depend on the extra conditions.

The coefficients A_{ij}, B_{ij} in solution (34) can be solved by

$$M \cdot C = P \tag{36}$$

where M is the coefficient matrix (35) for boundary conditions, $C = [A_{11}, A_{12}, \dots, A_{32}, B_{32}]$ is the coefficient vector to be solved and $P = [p_1, p_2, \dots, p_9, p_{10}]$ is a constant vector depending on the initial data. Note that only p_9, p_{10} and the last two lines of M depend on artificial tangential conditions.

According to the discussion above we need to prove A_{11}, A_{12} do not depend on the artificial tangential conditions. More precisely, we need to prove A_{11}, A_{12} do not depend on the last two lines of matrix M and p_9, p_{10} .

For convenience, we rewrite M into a block form

$$M = \begin{pmatrix} M_1(8 \times 2) & M_2(8 \times 8) \\ M_3(2 \times 2) & M_4(2 \times 8) \end{pmatrix} \quad (37)$$

We do the Gauss elimination for block M_2 and it shows that the rank of submatrix M_2 is 6 for any angle conditions. this means we can make the last two lines of M_2 be zeros by row deduction and meanwhile making the last two lines of M_1 into a full rank (2×2) matrix.

We again use M to denote the new matrix after row deduction. Next we compute M^{-1} in a block form satisfying

$$\begin{aligned} M \times M^{-1} &= \begin{pmatrix} M_1(8 \times 2) & M_2(8 \times 8) \\ M_3(2 \times 2) & M_4(2 \times 8) \end{pmatrix} \times \begin{pmatrix} \bar{M}_1(2 \times 8) & \bar{M}_2(2 \times 2) \\ \bar{M}_3(8 \times 8) & \bar{M}_4(8 \times 2) \end{pmatrix} \\ &= \begin{pmatrix} I(8 \times 8) & \mathbf{0} \\ \mathbf{0} & I(2 \times 2) \end{pmatrix} \end{aligned} \quad (38)$$

Expand directly to get

$$M_1 \times \bar{M}_1 + M_2 \times \bar{M}_3 = \mathbf{I}(8 \times 8) \quad (39)$$

$$M_1 \times \bar{M}_2 + M_2 \times \bar{M}_4 = \mathbf{0}(8 \times 2) \quad (40)$$

Note that (39)-(40) do not involve M_3, M_4 which means they do not depend on the artificial tangential conditions. If \bar{M}_1, \bar{M}_2 can be determined by equation (39)-(40) then we can say \bar{M}_1, \bar{M}_2 do not depend on the artificial conditions. The fact

$$\begin{pmatrix} A_{11} \\ A_{12} \end{pmatrix} = (\bar{M}_1 \quad \bar{M}_2) \times P$$

implies that A_{11}, A_{12} do not depend on the artificial conditions if we can further prove $\bar{M}_2 = \mathbf{0}$.

Actually, \bar{M}_1 can surely be solved from equation (39). This is because the last two lines of M_2 are zeros and we have exactly sixteen equations involving only the sixteen unknowns of \bar{M}_1 . For the same reason we can solve for \bar{M}_2 by equation (40). Actually, since the last two lines of M_1 is a full rank (2×2) matrix \bar{M}_2 must be zero. This completes the proof that the coefficients A_{11}, A_{12} in equation (33) do not depend on the artificial conditions. And consequently, the shapes of the three curves do not depend on the artificial tangential conditions. Novick-Cohen et al. [9] also pointed out that the artificial conditions do not influence the solutions, although the problem there is a little bit different. In [9] the authors look at a three phase problem in which all three interfaces evolve by minus the surface Laplacian of mean curvature and meet at a triple junction.

6 Numerical Discretization

Back to the full nonlinear problem, we present in detail the discretization procedure of the parabolic scheme (26) and junction conditions (27)-(31). The basic approach is to use a staggered grid in σ and we shall denote the approximations by capital letters with subscripts, i.e., $X_j(t) \simeq X((j-1/2)h, t) = (u((j-1/2)h, t), v((j-1/2)h, t))$ where h is grid spacing and $N = 1/h$ is the number of interior grid points for $\sigma \in [0, 1]$.

In order to write the discretized equations we introduce some additional notations. Let D_k denote the second order centered approximation of the k th derivative, i.e.,

$$\begin{aligned} D_1 X_j &= (X_{j+1} - X_{j-1})/2h \\ D_2 X_j &= (X_{j+1} + X_{j-1} - 2X_j)/h^2 \end{aligned}$$

and let D_+ and \mathcal{F} denote forward differencing and forward averaging, respectively,

$$\begin{aligned} D_+ X_j &= (X_{j+1} - X_j)/h \\ \mathcal{F} X_j &= (X_{j+1} + X_j)/2 \end{aligned}$$

We discretize each motion separately.

6.1 Grain Boundary Motion(Motion by Mean Curvature)

The grain boundary motion is approximated at all grid points by standard differences,

$$\dot{X}_j^i = \frac{D_2 X_j^i}{|D_1 X_j^i|^2} \quad i = 1, j = 1, 2, \dots, N \quad (41)$$

where \dot{X}_j stands for time derivative. Formally, these discrete equations require values of X_0 and X_{N+1} outside the computation domain. We shall use the boundary condition to extrapolate the interior values of X_1 and X_N to the unknown exterior values of X_0 and X_{N+1} . We shall give the details of the extrapolation procedure later.

6.2 Surface Diffusion

The higher order derivatives appeared in surface diffusion are approximated by

$$(X_{\sigma\sigma\sigma})_j \simeq D_3 X_j = \frac{D_2 X_{j+1} - D_2 X_{j-1}}{2h} \quad (42)$$

$$(X_{\sigma\sigma\sigma\sigma})_j \simeq D_4 X_j = \frac{D_2 X_{j-1} + D_2 X_{j+1} - 2D_2 X_j}{h^2} \quad (43)$$

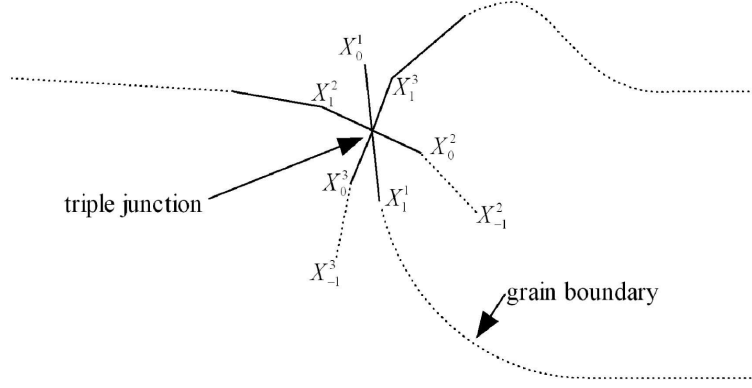


Figure 5: Sketch of the ghost points at the triple junction.

There are some other terms such as $S_\sigma, S_{\sigma\sigma}, S_{\sigma\sigma\sigma}$ to be approximated. Start from (11) and differentiate several times with respect to σ to get

$$\begin{aligned} S_\sigma &= \sqrt{u_\sigma^2 + v_\sigma^2} = |X_\sigma| \\ S_{\sigma\sigma} &= \frac{u_\sigma u_{\sigma\sigma} + v_\sigma v_{\sigma\sigma}}{\sqrt{u_\sigma^2 + v_\sigma^2}} = \frac{X_\sigma \cdot X_{\sigma\sigma}}{|X_\sigma|} \\ S_{\sigma\sigma\sigma} &= -\frac{(X_\sigma \cdot X_{\sigma\sigma})^2}{|X_\sigma|^3} + \frac{X_{\sigma\sigma} \cdot X_{\sigma\sigma} + X_\sigma \cdot X_{\sigma\sigma\sigma}}{|X_\sigma|} \end{aligned}$$

Every term in scheme (26) is now ready to be approximated by standard differences.

6.3 Junction Conditions at $\sigma = 0$

The discretization at the junction point is much more complicated. Since there are fourth order derivatives for the surface diffusion we shall need two ghost points for each surface curve and one ghost point for grain boundary. These ghost points are denoted by $X_0^1, X_{-1}^2, X_0^2, X_{-1}^3, X_0^3$ respectively. The junction conditions (27)-(31) are approximated as follows, see Fig. 5.

Condition (27),

$$\mathcal{F}X_0^1 = \mathcal{F}X_0^2 = \mathcal{F}X_0^3 = C \quad (44)$$

where C denotes the junction point.

The angle conditions (28)-(29) are approximated by

$$\frac{D_+ X_0^1}{|D_+ X_0^1|} \cdot \frac{D_+ X_0^2}{|D_+ X_0^2|} = \cos \theta_{12} \quad (45)$$

$$\frac{D_+ X_0^1}{|D_+ X_0^1|} \cdot \frac{D_+ X_0^3}{|D_+ X_0^3|} = \cos \theta_{13} \quad (46)$$

Discretize condition (30) for each surface curve to get

$$\frac{D_2 X_C^2 \cdot (D_1 X_C^2)^\perp}{|D_1 X_C^2|^3} = -\frac{D_2 X_C^3 \cdot (D_1 X_C^3)^\perp}{|D_1 X_C^3|^3} \quad (47)$$

Since staggered grid are used, center C is a midpoint not a grid points. But we still can use previous notations D_k with the following extensions

$$\begin{aligned} X_{C-1}^i &= (X_{-1}^i + X_0^i)/2 = \mathcal{F}X_{-1}^i \\ X_{C+1}^i &= (X_1^i + X_2^i)/2 = \mathcal{F}X_1^i \end{aligned}$$

κ_s can be expressed by

$$\kappa_s = \frac{X_{\sigma\sigma\sigma} \cdot X_\sigma^\perp}{|X_\sigma|^4} - 3 \frac{S_{\sigma\sigma}(X_{\sigma\sigma} \cdot X_\sigma^\perp)}{|X_\sigma|^5} \quad (48)$$

Thus condition (31) is approximated by

$$\frac{D_3 X_C^2 \cdot (D_1 X_C^2)^\perp}{|D_1 X_C^2|^4} - 3 \frac{S_{\sigma\sigma}^2(D_2 X_C^2 \cdot (D_1 X_C^2)^\perp)}{|D_1 X_C^2|^5} = \frac{D_3 X_C^3 \cdot (D_1 X_C^3)^\perp}{|D_1 X_C^3|^4} - 3 \frac{S_{\sigma\sigma}^3(D_2 X_C^3 \cdot (D_1 X_C^3)^\perp)}{|D_1 X_C^3|^5} \quad (49)$$

Finally, the artificial tangential conditions is calculated by

$$\frac{D_2 X_C^i \cdot D_1 X_C^i}{|D_1 X_C^i|^3} = 0 \quad \text{for } i = 2, 3 \quad (50)$$

We now finish discretizing the junction conditions.

6.4 Domain Boundary Conditions at $\sigma = 1$

The discretization at $\sigma = 1$ is straightforward.

$$\begin{aligned} \mathcal{F}X_N^i|_{t=n \cdot dt} &= \mathcal{F}X_N^i|_{t=(n-1) \cdot dt} \quad \text{for } i = 1, 2, 3 \\ D_+ X_N^i &= 0 \quad \text{for } i = 2, 3 \end{aligned}$$

7 Time Stepping

7.1 Explicit Scheme

As an explicit scheme, forward Euler method is used for the time stepping process.

$$X^{n+1} = X^n + \Delta t F(X^n) \quad (51)$$

Here $F(X^n)$ denotes the right hand side in formulation (25) evaluated at time level n . Time steps Δt are chosen so that the full discrete scheme is stable. Here we choose $\Delta t = 1e-12$. This scheme

is easy to implement. Given the results at time n we update the values of the interior grid points by forward Euler method to time level $n + 1$ for the three curves respectively. Next solve for the ghost points, junction point and the boundary points by the boundary conditions. Then go on to the next time level. The time step is excessively small due to the stiffness of the fourth order parabolicity as noted previously.

7.2 Implicit Scheme

In order to avoid the excessively small time steps for explicit scheme we consider implicit techniques in this section. For simplicity we use backward Euler method. Given the values at time n we update the values at time level $n + 1$ by solving the nonlinear system

$$X^{n+1} - \Delta t F(X^{n+1}) - X^n = 0 \quad (52)$$

Since the three curves are strongly coupled by the junction, we solve all unknown points simultaneously including the ghost points and the extrapolated boundary points. This leads to a large nonlinear system which is solved by Newton's method. There is no doubt that this scheme should be stable for any time steps. But it can not survive a long time computation due to the nonuniform tangential velocity which leads to a nonuniform distribution of the grid points. This phenomenon can not be fixed even if we refine the grid.

One way to overcome this difficulty is regriding the grid points once they become too far or too close. But the bad distribution could happen only near the junction and the closer to the junction the sparser (or denser) the grid points are. Hence it is hard to regrid no matter globally or locally. Another way is adjusting the tangential velocity of the grid points such that they could adjust themselves being uniform. And this is the motivation for the next section.

Numerical results for scheme (26) with time step $\Delta t = 1e - 4$ are shown in Fig. 6. All numerical experiments in this paper start from the same position as showed in Fig. 6. All results are compared with a travelling wave solution solved by Amy et al [11].

8 Adjustment of Tangential Velocity

We have mentioned that long time computations are problematical even for implicit schemes. This is because of the bad distribution of grid points. To get a more uniform distribution of grid points along the curve we consider adding an artificial term to adjust the tangential velocity of the grid points for the motion by surface diffusion.

We consider the following modified scheme for the fourth order problem

$$X_t = F(X) + \alpha \left(\frac{X_{\sigma\sigma\sigma\sigma}}{|X_\sigma|^4} \cdot \vec{t} \right) \vec{t} \quad (53)$$

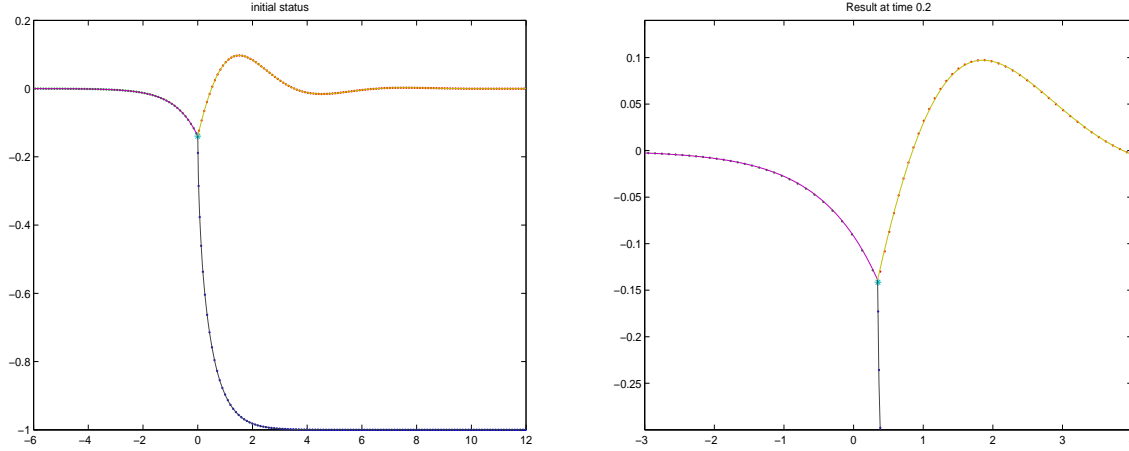


Figure 6: Plot of results for scheme (26) with backward Euler method for a short time with $m = 0.5$. Left: initial status with grid points; Right: result zoomed in near triple junction. Dotted line: numerical solution; Solid line: travelling wave solution; Time step size: $\Delta t = 1e - 2$.

where α is a constant to be determined. The newly added term in (53) will not influence the normal velocity but it does change the tangential velocity. We do not know exactly how to choose the optimal α but $\alpha = -100$ seems to work well for our problem. The result is shown in Fig.7. It is obvious that the grid points are much more uniform than that in Fig.6. The time step size for Fig.7 is $\Delta t = 0.01$. A numerical convergence study is shown in Table 1.

dt	Δs	L_2 Norm	Rate	L_∞ Norm	Rate
$dt = 0.01\Delta s^2$	0.2	3.1494e-04		2.0241e-03	
	0.1	7.9775e-05	1.9811	5.4797e-04	1.8852
	0.05	2.1445e-05	1.8953	1.4530e-05	1.9151

Table 1: Estimated errors and convergence rates for parabolic formulation with $m = 0.5$. Errors are evaluated at $t = 0.02$.

Although the newly added tangential term improves the numerical behavior it can not completely overcome the difficulty. The artificial tangential conditions discussed in section 5 make the problem even more complicated. All these motivate us to seek a more efficient scheme.

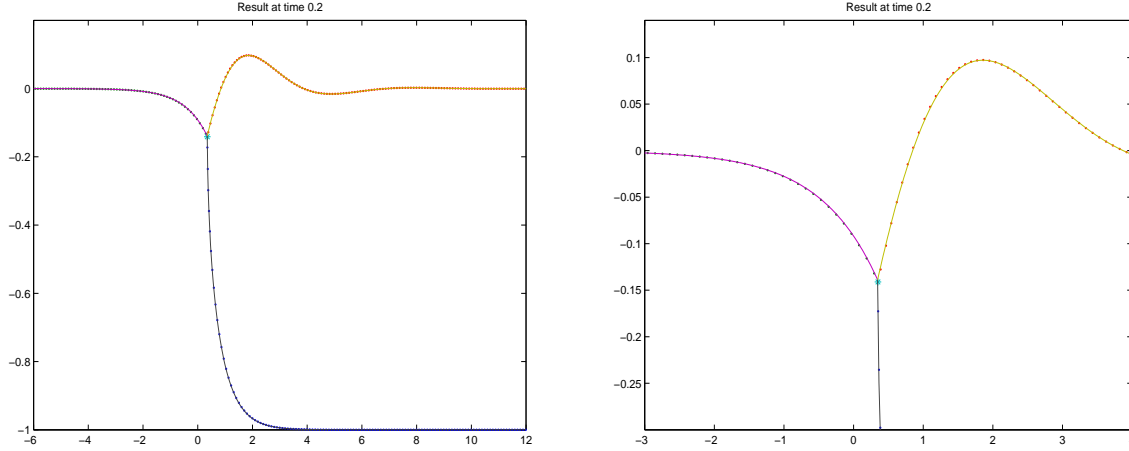


Figure 7: Plot of the results for scheme (53) with $m = 0.5, \alpha = -100, \Delta t = 0.01$. Left: result at $t=0.2$; Right: result zoomed in near triple junction at $t=0.2$. Dotted line: numerical result; Solid line: travelling wave solution.

Remark There is another way to adjust the tangential velocity,

$$X_t = F(X) + \alpha \left(\frac{X_{\sigma\sigma}}{|X_\sigma|^2} \cdot \vec{t} \right) \vec{t} \quad (54)$$

For this case, we should choose α positive, for example $\alpha = 100$.

9 A PDAE Formulation

As we have pointed out in section 8, the fully parabolic scheme (26) does not always have good numerical behavior. And the presence of the artificial tangential condition makes the discretization of the original problem more complicated. In this section we propose another formulation that can overcome these disadvantages and also avoids possible loss of tangential monotonicity in the parametrization due to the fourth order PDE.

Let us again start from the motion by mean curvature. First of all the basic evolution law should be satisfied, i.e.,

$$X_t \cdot \vec{n} - \kappa = 0 \quad (55)$$

Because there are two free variables in this equation we need one more equation for solvability. Since the requirement for the normal direction motion has been fulfilled by equation (55) we use the second equation to impose a constraint on the distribution of grid points. It is natural to let

all grid points have equal spaces. To avoid introducing an extra variable we let the change rate between any two adjacent spaces is zero, i.e.,

$$|X_\sigma|_\sigma = 0 \quad (56)$$

Note that

$$|X_\sigma|_\sigma = (\sqrt{X_\sigma \cdot X_\sigma})_\sigma = \frac{X_\sigma \cdot X_{\sigma\sigma}}{|X_\sigma|}$$

the following equations are actually used to describe the motion and keep grids equi-spaced,

$$\begin{aligned} X_t \cdot \vec{n} - \kappa &= 0 \\ X_\sigma \cdot X_{\sigma\sigma} &= 0 \end{aligned}$$

These are called partial differential algebraic equations (PDAEs).

In a similar way we derive the PDAEs for the motion by surface diffusion,

$$\begin{aligned} X_t \cdot \vec{n} + \kappa_{ss} &= 0 \\ X_\sigma \cdot X_{\sigma\sigma} &= 0 \end{aligned}$$

Then the full PDAE system for the coupled motion is

$$\begin{aligned} X_t^1 \cdot \vec{n} - \kappa &= 0 \\ X_t^2 \cdot \vec{n} + \kappa_{ss} &= 0 \\ X_t^3 \cdot \vec{n} + \kappa_{ss} &= 0 \\ X_\sigma^i \cdot X_{\sigma\sigma}^i &= 0 \quad i = 1, 2, 3 \end{aligned} \quad (57)$$

The boundary conditions are the same as the parabolic case except that we do not need artificial tangential conditions any more.

This is an implicit index-1 DAE system. Usually an index-1 DAE can be discretized directly without any numerical difficulties [1], and that is our experience in this case.

Although the boundary conditions are the same as those of the parabolic system, the discretization is a little bit different. Instead of using five ghost points we now introduce only three ghost points plus two extra variables which stand for the curvature at the two ghost points corresponding to the two surface branches. The two variables are denoted by κ_0^2, κ_0^3 and the last two junction conditions are approximated by

$$\begin{aligned} \frac{\kappa_0^2 + \kappa_1^2}{2} &= -\frac{\kappa_0^3 + \kappa_1^3}{2} \\ \frac{(\kappa_0^2 - \kappa_1^2)}{|D_1 X_c^2|} &= \frac{(\kappa_0^3 - \kappa_1^3)}{|D_1 X_c^3|} \end{aligned}$$

where κ_1^i stands for the curvature of the first interior point of curve i and we use the average of κ_0^i, κ_1^i to approximate the curvature at the center point, i.e., junction point. Again the sign should be carefully handled.

Implementing this scheme one obtains a better result shown in Fig.8. The result is much more accurate and the grid points are more uniform as well. An error comparison is shown in Table 2. A numerical convergence study of the PDAE formulation is shown in Table 3. The convergence rates shown in Table 3 are close to 2 as expected.

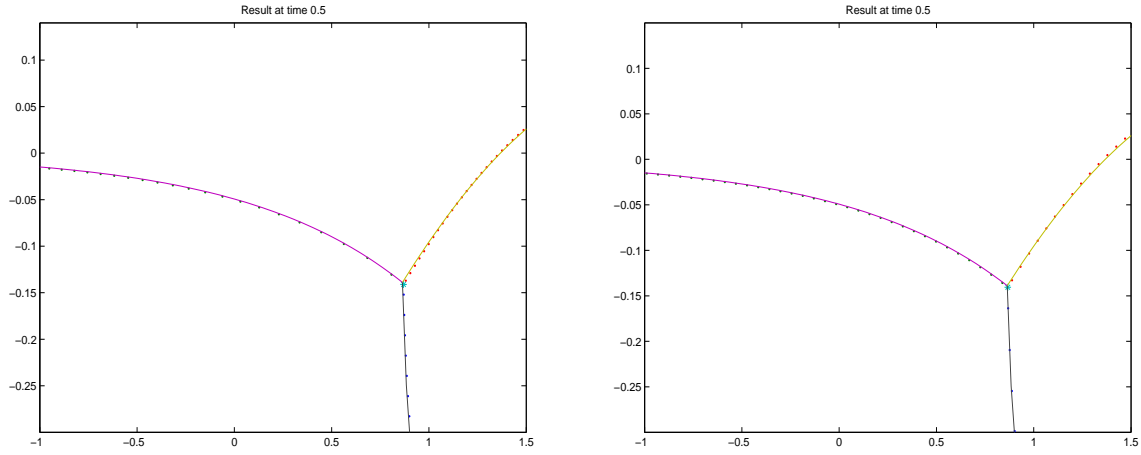


Figure 8: Results comparison between the two schemes. Left: result for (26); Right: result for (57). Both pictures are zoomed in near triple junction. Dotted line: numerical solution; Solid line: travelling wave solution; Time step size: $\Delta t = 0.01$.

	Parabolic Formulation	PDAE Formulation
Δs	0.05	0.05
Δt	0.01	0.01
L_∞	0.0041	0.0027

Table 2: Performance of the two formulations with L_∞ norm and $\Delta t = 0.01$.

Without difficulty we can apply this scheme to the case when the surface curve is not a single-valued function as shown in Fig.9

dt	Δs	L_2 Norm	Rate	L_∞ Norm	Rate
$dt = 0.01\Delta s^2$	0.2	2.7837e-04		1.8996e-03	
	0.1	7.2717e-05	1.9366	5.4444e-04	1.8029
	0.05	1.8732e-05	1.9568	1.4732e-04	1.8858

Table 3: Estimated errors and convergence rates for PDAE formulation with $m = 0.5$. Errors are evaluated at $t = 0.02$.

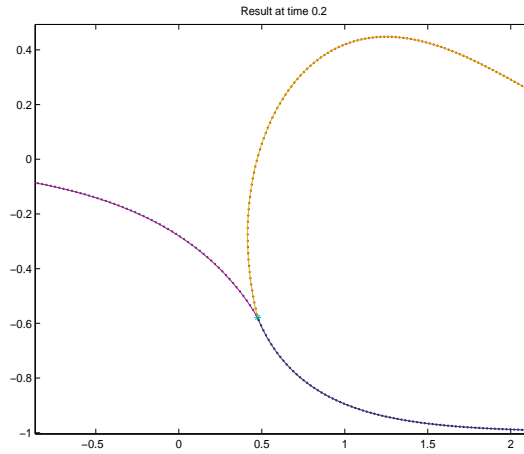


Figure 9: Plot of the results for scheme (57) with $m = 1.96$ which has non-single valued upper surface. Dotted line: numerical result; Solid line: travelling wave solution.

10 An Example of Surface Diffusion Problem

We temporally move our focus to a normal direction motion that involves only motion by surface diffusion. The motion starts with a closed star shaped curve and evolves with a speed equal to the second derivative of curvature with respect to arc length. According to the properties of surface diffusion the curve will evolve into a circle and preserve the area enclosed by itself. This problem is computed using the PDAE formulation for the surface diffusion and the result is shown in Fig.10. The method conserves the area quite well and the change is about 0.032%. Similar examples have been investigated using level set methods in [5, 14]. Level set methods have unbeatable superiority for interface motion problem especially when there is topology change. But for this simple problem (with no topology change) our method is more efficient and accurate. Note that this problem can also be computed by the parabolic formulation.

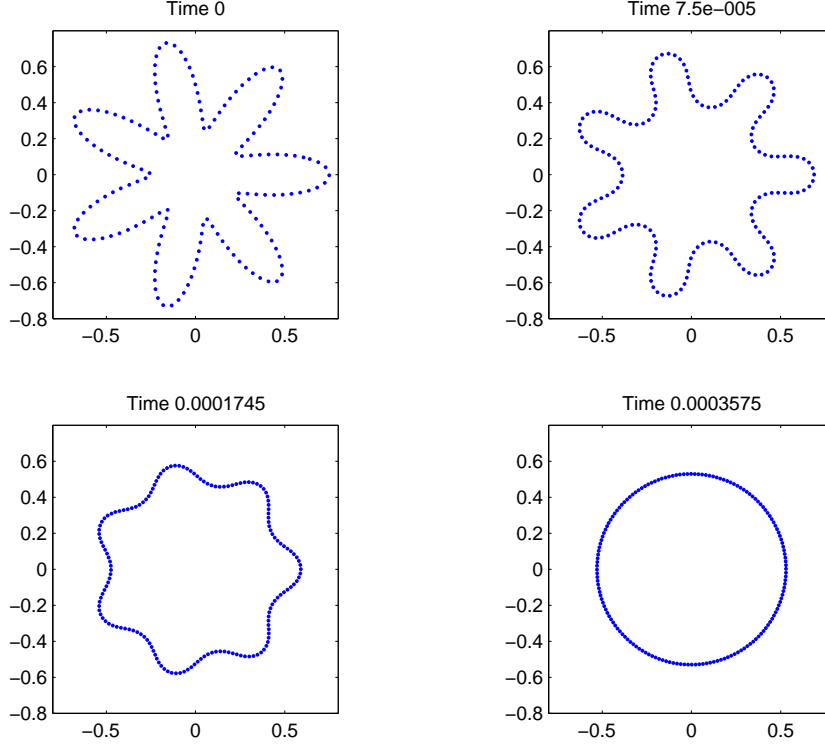


Figure 10: A computational example that involve only the motion by surface diffusion. $\Delta t = 5 \times 10^{-7}$. The area changes by 0.032%

11 Well-posedness for the PDAE System

Similar to the parabolic system we do a well-posedness analysis for the PDAE system in this section.

Considering the same linear problem as that in section 5.1 one obtains

$$\begin{aligned}
 X_t^1 \cdot d_1^\perp &= X_{\sigma\sigma}^1 \cdot d_1^\perp \\
 d_1 \cdot X_{\sigma\sigma}^1 &= 0 \\
 X_t^2 \cdot d_2^\perp &= -X_{\sigma\sigma\sigma\sigma}^2 \cdot d_2^\perp \\
 d_2 \cdot X_{\sigma\sigma}^2 &= 0 \\
 X_t^3 \cdot d_3^\perp &= -X_{\sigma\sigma\sigma\sigma}^3 \cdot d_3^\perp \\
 d_3 \cdot X_{\sigma\sigma}^3 &= 0
 \end{aligned} \tag{58}$$

where d_i and d_i^\perp stand for unit tangential direction and unit normal direction of the i^{th} curve respectively.

Linearization of the boundary conditions are exactly the same as before. They differ only for the discretization procedure.

If $d_{i1}, d_{i2} \neq 0$ the linearized system (58) has solution in the form

$$\begin{cases} u_1 = A_{11}e^{-\sqrt{s}\sigma} + B_{11} \\ v_1 = -k_1 A_{11}e^{-\sqrt{s}\sigma} + \frac{1}{k_1} B_{11} \\ u_2 = A_{21}e^{\lambda_1\sigma} + B_{21}e^{\lambda_2\sigma} + C_{21} \\ v_2 = -k_2(A_{22}e^{\lambda_1\sigma} + B_{22}e^{\lambda_2\sigma}) + \frac{1}{k_2} C_{21} \\ u_3 = A_{31}e^{\lambda_1\sigma} + B_{31}e^{\lambda_2\sigma} + C_{31} \\ v_3 = -k_3(A_{32}e^{\lambda_1\sigma} + B_{32}e^{\lambda_2\sigma}) + \frac{1}{k_3} C_{31} \end{cases} \quad (59)$$

where $k_i = \frac{d_{i1}}{d_{i2}}$ is a constant and

$$\lambda_1 = \left(-\frac{\sqrt{2}}{2} + \frac{\sqrt{2}}{2}i\right)\sqrt[4]{s} \quad \lambda_2 = \left(-\frac{\sqrt{2}}{2} - \frac{\sqrt{2}}{2}i\right)\sqrt[4]{s}$$

Without changing the well-posedness of the problem we specify one of the tangential directions, say $d_1 = (0, -1)^T$. Further we assume

$$\theta_{12}, \theta_{13} \in (0, \pi) \text{ and } \theta_{12}, \theta_{13} \neq \frac{\pi}{2}$$

Since $d_{11} = 0$ now the solution is changed to

$$\begin{cases} u_1 = A_{11}e^{-\sqrt{s}\sigma} \\ v_1 = B_{11} \\ u_2 = A_{21}e^{\lambda_1\sigma} + B_{21}e^{\lambda_2\sigma} + C_{21} \\ v_2 = -k_2(A_{22}e^{\lambda_1\sigma} + B_{22}e^{\lambda_2\sigma}) + \frac{1}{k_2} C_{21} \\ u_3 = A_{31}e^{\lambda_1\sigma} + B_{31}e^{\lambda_2\sigma} + C_{31} \\ v_3 = -k_3(A_{32}e^{\lambda_1\sigma} + B_{32}e^{\lambda_2\sigma}) + \frac{1}{k_3} C_{31} \end{cases} \quad (60)$$

Apply these solutions to boundary conditions to get an 8×8 matrix M and compute the determinant of M directly to get

$$|M| = \frac{4\sqrt{2}s^{7/4} \sin(\theta_{12} + \theta_{13}) - 8s^2(\sin \theta_{12} + \sin \theta_{13})}{\cos^2 \theta_{12} \cos^2 \theta_{13}}$$

For the special case when one of the angles θ_{12}, θ_{13} is $\frac{\pi}{2}$, for example, $\theta_{12} = \frac{\pi}{2}$,

$$\begin{cases} u_1 = A_{11}e^{-\sqrt{s}\sigma} \\ v_1 = B_{11} \\ u_2 = C_{21} \\ v_2 = A_{22}e^{\lambda_1\sigma} + B_{22}e^{\lambda_2\sigma} \\ u_3 = A_{31}e^{\lambda_1\sigma} + B_{31}e^{\lambda_2\sigma} + C_{31} \\ v_3 = -k_3(A_{32}e^{\lambda_1\sigma} + B_{32}e^{\lambda_2\sigma}) + \frac{1}{k_3} C_{31} \end{cases} \quad (61)$$

The determinant of the coefficient matrix is

$$|M| = \frac{-8s^2 \sin \theta_{13} + 4\sqrt{2}s^{7/4} \cos \theta_{13} - 8s^2}{\cos^2 \theta_{13}}$$

And if both θ_{12}, θ_{13} are $\frac{\pi}{2}$,

$$\begin{cases} u_1 = A_{11}e^{-\sqrt{s}\sigma} \\ v_1 = B_{11} \\ u_2 = C_{21} \\ v_2 = A_{22}e^{\lambda_1\sigma} + B_{22}e^{\lambda_2\sigma} \\ u_3 = C_{31} \\ v_3 = A_{32}e^{\lambda_1\sigma} + B_{32}e^{\lambda_2\sigma} \end{cases} \quad (62)$$

The corresponding determinant of the matrix M is

$$|M| = -16s^2$$

Similar as before all cases discussed above are well-posed if $0 < \theta_{12}, \theta_{13} < \pi$ and $\theta_{12} + \theta_{13} \geq \pi$. Note that the well-posedness property here coincides with that for the parabolic system we got before.

12 Conclusion

We proposed two formulations to describe the coupled surface and grain boundary motion. Both of them are well-posed and easy to be implemented by finite difference method. Numerical results are shown to be accurate. The PDAE formulation behaves better than the parabolic form does. And since all grid points are equispaced for the PDAE formulation it is convenient to regrid globally when necessary. This often happens when the curves expand or shrink quickly.

It is obvious that these schemes can also be used to simulate the motion of a curve that involves only mean curvature motion or surface diffusion as shown in section 10. And they are extensible to any normal direction motion. Wherever applicable these methods are more efficient comparing to the level set methods. But they can not manage topology changes during the evolution.

Acknowledgements

The authors would like to thank Amy Novick-Cohen for the helpful information on recent progress about the model addressed in this paper.

Appendix A: Reformulation of the Motion.

The original curvature motion and surface diffusion are given as

$$\begin{aligned} V_c &= A\kappa \\ V_d &= -B\kappa_{ss} \end{aligned}$$

Without loss of generality will shall prove in particular in a parameterized form that we may normalize both A and B by rescaling the time and space.

Suppose the original motions are modelled by

$$\begin{aligned} X_t \cdot \vec{n} &= A\kappa \\ Y_t \cdot \vec{n} &= -B\kappa_{ss} \end{aligned} \tag{63}$$

We first rescale the time by

$$\tilde{t} = Tt$$

Then equation (63) becomes

$$\begin{aligned} X_{\tilde{t}} \cdot \vec{n} &= \frac{A}{T}\kappa \\ Y_{\tilde{t}} \cdot \vec{n} &= -\frac{B}{T}\kappa_{ss} \end{aligned} \tag{64}$$

The spatial variable X, Y are rescaled as

$$\tilde{X} = RX, \quad \tilde{Y} = RY$$

And we can easily verify that

$$\tilde{s} = Rs$$

where \tilde{s} is the arc length in the new system. More derivation shows that

$$\tilde{X}_{\tilde{s}} = X_s, \quad \tilde{Y}_{\tilde{s}} = Y_s, \quad \tilde{\kappa} = \frac{1}{R}\kappa, \quad \tilde{\kappa}_{\tilde{s}\tilde{s}} = \frac{1}{R^3}\kappa_{ss}$$

Now equation (64) becomes

$$\begin{aligned} \tilde{X}_{\tilde{t}} \cdot \vec{n} &= \frac{AR^2}{T}\tilde{\kappa} \\ \tilde{Y}_{\tilde{t}} \cdot \vec{n} &= -\frac{BR^4}{T}\tilde{\kappa}_{\tilde{s}\tilde{s}} \end{aligned} \tag{65}$$

Here we use the same notation \vec{n} since the normal direction does not change. If we choose

$$R = \sqrt{\frac{A}{B}}, \quad T = \frac{A^2}{B}$$

then equation (65) becomes

$$\begin{aligned} \tilde{X}_{\vec{t}} \cdot \vec{n} &= \tilde{\kappa} \\ \tilde{Y}_{\vec{t}} \cdot \vec{n} &= -\tilde{\kappa}_{\vec{s}\vec{s}} \end{aligned} \tag{66}$$

This complete the normalization of coefficients A and B .

Appendix B: Proof of Equation (18)

One has the following fact

$$X_{ss} \cdot X_{ss} = \kappa^2 \tag{67}$$

Differentiating (67) with respect to s one obtains

$$X_{sss} \cdot X_{ss} = \kappa \kappa_s$$

$$X_{ssss} \cdot X_{ss} + X_{sss} \cdot X_{sss} = \kappa \kappa_{ss} + \kappa_s^2$$

Then an expression for κ_{ss} can be derived,

$$\kappa_{ss} = \frac{X_{ssss} \cdot X_{ss} + X_{sss} \cdot X_{sss} - \kappa_s^2}{\kappa} \tag{68}$$

On the other hand, one has

$$X_{ss} = \kappa \vec{n}$$

Take derivative again and calculate the inner product of X_{sss}

$$X_{sss} = \kappa_s \vec{n} + \kappa \vec{n}_s = \kappa_s \vec{n} - \kappa^2 \vec{t}$$

$$X_{sss} \cdot X_{sss} = \kappa_s^2 + \kappa^4 \tag{69}$$

Substitute equation (69) into (68) to get

$$\kappa_{ss} = X_{ssss} \cdot \vec{n} + \kappa^3 \tag{70}$$

Using equation (70) together with the fact that

$$\kappa^2 X_{ss} \cdot \vec{n} = \kappa^2 (X_{ss} \cdot \vec{n}) = \kappa^3 \tag{71}$$

one obtains

$$\kappa_{ss} = (X_{ssss} + \kappa^2 X_{ss}) \cdot \vec{n}$$

which completes the proof.

References

- [1] Uri M. Ascher and Linda R. Petzold *Computer methods for ordinary differential equations and differential-algebraic equations* SIAM, (1998), 231-279.
- [2] Lia Bronsard, Fernando Reitich *On three-phase boundary motion and the singular limit of a vector-valued Ginzburg-Landau equation* Archive for Rational Mechanics and Analysis, vol 124, no 4, (1993), 355-379.
- [3] Lia Bronsard and Brian T.R. Wetton *A numerical method for tracking curve networks moving with curvature motion* Journal of Computational Physics 120, (1995),66-87.
- [4] J. Cahn and J. Taylor, *Overview 113: Surface motion by surface diffusion*, Acta Metallurgica et Materialia, 42 (1994), 1045-1063.
- [5] David L. Chopp and J.A. Sethian, *Motion by intrinsic laplacian of curvature*, Interfaces and Free Boundaries 1 (1999),1-18.
- [6] Dunn CG, Daniels FW, Bolton MJ, Trans. Am. Inst. Min. Engrs, 185 (1949), 708.
- [7] Harald Garcke and Amy Novice-Cohen, *A singular limit for a system of degenerate cahn-hilliard equations*, Advanced Differential Equations, 5 (2000), 401-434.
- [8] Jacob Kanel and Amy Novick-Cohen, *Coupled surface and grain boundary motion: nonclassical traveling wave solutions* Advanced Differential Equations. 9 (2004), 299-327.
- [9] Jacob Kanel, Amy Novick-Cohen and Arkady Vilenkin *A numerical study of grain boundary motion in bicrystals* Acta Materialia 53 (2005), 227-235.
- [10] Jacob Kanel, Amy Novick-Cohen and Arkady Vilenkin *A traveling wave solution for coupled surface and grain boundary motion* Acta Materialia 51 (2003), 1981-1989.
- [11] Jacob Kanel, Amy Novick-Cohen and Arkady Vilenkin *Coupled surface and grain boundary motion:a travelling wave solution*. Nonlinear Analysis 59 (2004), 1267-1292.
- [12] Donghong Min, Harris Wong, *A model of migrationg grain-boundary grooves with application to two mobility-measurement methods* Acta Materialia 50 (2002), 5155-5169.
- [13] W.W. Mullins, *Theory of thermal grooving*, Journal of Applied Physics, 28 (1957), 333-339.
- [14] Peter Smereka *Semi-Implicit level set methods for curvature and surface diffusion motion* Journal of scientific computing, Vol 19, Nos. 1-3 (2003), 439-456.
- [15] V.A. Solonnikov, *Boundary value problems in physics*, Proceedings of the Steklov Institute, Providence, R.I., Vol. LXXXIII, (1965), 487-491.